Contents lists available at ScienceDirect

Chemical Physics

Exciton dynamics in a disordered conjugated polymer: Three-pulse photon-echo and transient grating experiments

J. Sperling [a], A. Nemeth [a], P. Baum [a,b], F. Šanda [c], E. Riedle [b], H.F. Kauffmann [a,*], S. Mukamel [d], F. Milota [a]

[a] *Department of Physical Chemistry, University of Vienna, Währingerstrasse 42, 1090 Vienna, Austria*
[b] *Chair for BioMolecular Optics, Ludwig-Maximilians-University (LMU), Oettingenstrasse 67, 80538 Munich, Germany*
[c] *Institute of Physics, Faculty of Mathematics and Physics, Charles University, Ke Karlovu 5, Prague 121 16, Czech Republic*
[d] *Department of Chemistry, University of California, Irvine, CA 92697-2025, United States*

ABSTRACT

We study the sub-picosecond exciton dynamics of the prototypical soluble conjugated polymer poly[2-(2′-ethylhexyloxy)-5-methoxy-1,4-phenylenevinylene] (MEH-PPV) by comparative three-pulse photon-echo peak-shift and transient grating measurements, performed under excitation energy tuning conditions. The strong sensitivity of signal decays to the chosen excitation energy is ascribed to the interplay of inter- and intra-segmental relaxation events in an ensemble of electronically coupled sites. As a result, the energetic site-to-site disorder and its contribution to the spectral lineshape is most reliably determined for excitation of the redmost part of the absorption spectrum. Comparing the data for the two solvents toluene and tetrahydrofurane, we conclude a weak sensitivity only to the specific type of solute-solvent interactions. Within our time-resolution, we surprisingly recover weak but reproducible modulations of the third-order signals that are damped out on the early picosecond timescale.

© 2008 Elsevier B.V. All rights reserved.

1. Introduction

The molecular exciton model has been quite successful in explaining the main spectral features of conjugated polymers [1,2]. It rests upon the assumption of finite conjugation lengths along the polymer chain, due to a distribution of structural defects, and accordingly treats the polymer as a collection of segmental sub-units over which optical excitations are delocalized (hence the term spectroscopic units). In this picture, inter-segmental electronic couplings allow excitons to move along the chain towards sites of lower energy. The optical response is thus determined by static disorder (the spectral inhomogeneity of the site distribution), dynamic disorder (site-specific interactions with the bath), and excitation energy transfer (EET) processes. Detailed information on the interplay of these contributions remains hidden in the linear absorption spectrum of conjugated polymers, which usually consists of a single broad feature.

Time-resolved non-linear experiments are capable to provide a more detailed understanding of the lineshape of an assembly of coupled molecular chromophores [3,4]. Apart from an earlier photon-echo (PE) study on oriented films of polydiacetylene [5],

Scholes et al. [6] were the first who performed PE experiments on poly[2-(2′-ethylhexyloxy)-5-methoxy-1,4-phenylenevinylene] (MEH-PPV), which serves as a typical model for ground-state non-degenerate polymers of the poly(arylenevinylene) type (cf. Fig. 1). In some analogy to the situation encountered in molecular aggregates, the structureless electronic absorption of MEH-PPV has been explained to be dominated by bath-mediated exciton scattering [6]. It was argued that, due to fluctuations of site-to-site couplings between strongly coupled units, optical excitons sample over eigenenergies within about 50 femtoseconds (fs), precluding any significant contribution from static disorder to the absorption lineshape. On the other hand, the data of more recent, closely related three-pulse photon-echo peak-shift (3-PEPS) studies [7,8], could not be explained satisfactorily without considering a residual spectral inhomogeneity arising from conformational disorder of the polymer chain.

This state of affairs motivated the present contribution, in which we report systematic 3-PEPS and transient grating (TG) measurements on MEH-PPV in the two solvents toluene and tetrahydrofurane (THF). Tuning the central energies of sub-30 fs excitation pulses across the polymer absorption band, we observe a gradual change in the shape of both nonlinear signals. This allows to differentiate between inter- and intra-segmental relaxation events, the latter observable at increasingly site-selective excitation conditions (at low excitation energies).

* Corresponding author.
  E-mail addresses: jaroslaw.sperling@univie.ac.at (J. Sperling), harald.f.kauffmann@univie.ac.at (H.F. Kauffmann), franz.milota@univie.ac.at (F. Milota).
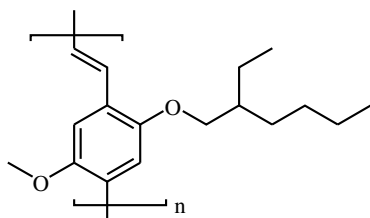
Fig. 1. Molecular structure of poly[2-(2′-ethylhexyloxy)-5-methoxy-1,4-phenylenevinylene] (MEH-PPV). Alkyloxy-chains attached to the conjugated poly(p-phenylenevinylene) (PPV) backbone facilitate solubility in common organic solvents.

2. Conceptual framework

In a third-order time-resolved experiment, three laser pulses (with wavevectors $\mathbf{k}_1$, $\mathbf{k}_2$, and $\mathbf{k}_3$) interact with the sample and create a nonlinear polarization $P^{(3)}$ that radiates the signal in a particular direction determined by phase-matching conditions. The third-order polarization $P^{(3)}$ is determined by the incoming electric fields and the third-order response function $S^{(3)}(\tau, T, t)$ of the system (we use τ and T to denote the first and second time interval between the three interactions, and t the time elapsed after the third interaction, respectively). $S^{(3)}$ can be obtained by a perturbative expansion of the system density matrix in the total electric field [3,4,9].

Since a comprehensive discussion of the underlying theory is beyond the scope of this work, we give an intuitive picture only for understanding of the main aspects to be discussed below. In a photon-echo experiment, the first pulse ($\mathbf{k}_1$) creates a coherence (i.e. a superposition) between the ground and excited state of an electronic absorber. The second pulse ($\mathbf{k}_2$, after time τ) converts the evolving coherence into population-space, creating a spatially periodic population grating of ground/excited states in the sample, which can undergo relaxation and wavepacket motion during the time interval T. The third pulse ($\mathbf{k}_3$), again, creates a superposition of states (evolving with an inverted phase), that radiates into the signal direction ($\mathbf{k}_s = -\mathbf{k}_1 + \mathbf{k}_2 + \mathbf{k}_3$). All signals to be discussed are measured in (time-integrated) homodyne detection mode. Assuming the impulsive limit the photon-echo signal intensity is then given by

$$I(\tau, T) \propto \int_0^\infty dt |S^{(3)}(\tau, T, t)|^2. \tag{1}$$

The 3-PEPS method is based on the following scanning-scheme. In each sequence, for a particular (fixed) population time delay T, the coherence time τ is scanned and the position of the maximum of $I(\tau, T)$ is evaluated along the τ-axis. The magnitude of this peak-shift τ^* (deviation from $\tau = 0$) is recorded for a selected range of population times, to give a plot of τ^* vs. T (the peak-shift decay). The popularity of the experiment results from the fact that, at not too short population time delays, the 3-PEPS signal of a chromophore ensemble reflects the (ensemble averaged) correlation function [10–12]

$$M(t) = \frac{\langle \delta\omega_{eg}(t)\delta\omega_{eg}(0) \rangle}{\langle \delta\omega_{eg}^2 \rangle} \tag{2}$$

of the individual fluctuations $\delta\omega_{eg}^i(t)$ in the electronic transition energies. Simply speaking, the 3-PEPS decay measures to what extent electronic frequencies of the system correlate on a time set by delay T. This property is particularly useful in the condensed phase, where the separation of timescales (and homogeneous and inhomogeneous contributions to the spectral lineshape) is not distinct. Thus, the method not only has been extensively used for stud-

ies of solvation dynamics on various model dyes [13,14], but also has shown to be a sensitive probe for tracing excitation energy transfer in multi-chromophore systems, like J-aggregates [15] or light-harvesting complexes [16,17].

Since the intensity of the echo signal does not enter into the 3-PEPS decay, we complement the data with transient grating measurements to gain additional information on the population dynamics during T. In TG experiments, the coherence time is fixed at $\tau = 0$ and the population time scanned through the region of interest. In the impulsive limit, the TG signal intensity is given by

$$I(T) \propto \int_{-\infty}^\infty dt |S^{(3)}(\tau = 0, T, t)|^2. \tag{3}$$

3. Experimental details

MEH-PPV is purchased from American Dye Source and used as delivered. Solutions (20 mg/100 ml) in toluene and THF (both from Merck, Uvasol grade) are prepared by sonicating for several hours at elevated temperatures and subsequent filtration to remove insoluble residues. Steady-state absorption and fluorescence spectra are recorded with a miniature fiberoptic spectrometer (Ocean Optics USB 2000).

A regenerative Ti:Sapphire amplifier system (RegA 9050-system, Coherent Inc.) generates 45 fs pulses at 800 nm with a repetition rate of 200 kHz, which are used to pump a noncollinear optical parametric amplifier (NOPA) that delivers sub-30 fs pulses tunable across the visible [18]. The NOPA-output passes a sequence of fused silica prisms for pulse compression and pre-compensation of dispersive elements. Three beams of equal intensity (10 nJ/pulse at the sample position) and dispersion are prepared by broadband beamsplitters and anti-reflection coated glass substrates of the same material and thickness. Two of the beams ($\mathbf{k}_2$ and $\mathbf{k}_3$) are delayed by motorized linear stages with a resolution of 0.1 μm. All three beams are aligned in parallel as an equilateral triangle (1 cm each side) and focused onto the sample to a common spot size of 200 μm by means of a 20 cm focal-length lens. To avoid photo-degradation of the sample a total volume of 100 ml of the respective solution is circulated through a 200 μm flow-cell.

Since even small amounts of chirp can have significant effects on third-order signals (see, e.g., Ref. [19]), attention is given to eliminate any higher-order dispersion. To that end, the excitation pulses are characterized by zero-additional-phase spectral phase interferometry for direct electric-field reconstruction [20,21] (ZAP-SPIDER). With ZAP-SPIDER, the amplitude and phase of a pulse can be characterized directly at the interaction point of the experiment. By optimizing the prism compressor for lowest material insertion, shortest pulses can be generated with negligible satellites from higher-order chirp. In the present experiments, pulse durations of 28 fs with more than 95% of the energy contained in a single main pulse are routinely achieved. Pulse lengths are further cross checked by intensity autocorrelation in a 50 μm thick β-Barium-Borate (BBO) crystal placed at the sample position.

All third-order signals are spatially filtered and detected by photodiodes in combination with lock-in amplifiers. Two-pulse photon-echoes are used to determine $\tau = 0$ and $T = 0$ with high precision. Three-pulse photon-echoes and TG signals are simultaneously measured in the two directions $\mathbf{k}_s = -\mathbf{k}_1 + \mathbf{k}_2 + \mathbf{k}_3$ and $\mathbf{k}_s' = \mathbf{k}_1 - \mathbf{k}_2 + \mathbf{k}_3$, which is done to check consistency of the TG data and to determine the peak-shift with greater precision (by Gaussian fitting of the signals and halving the temporal separation of the maxima). A typical sequence of 3-PEPS measurements is shown in Fig. 2. Testing against other fitting schemes (parabolic and higher polynomial), we observe no significant changes in the 3-PEPS decays.
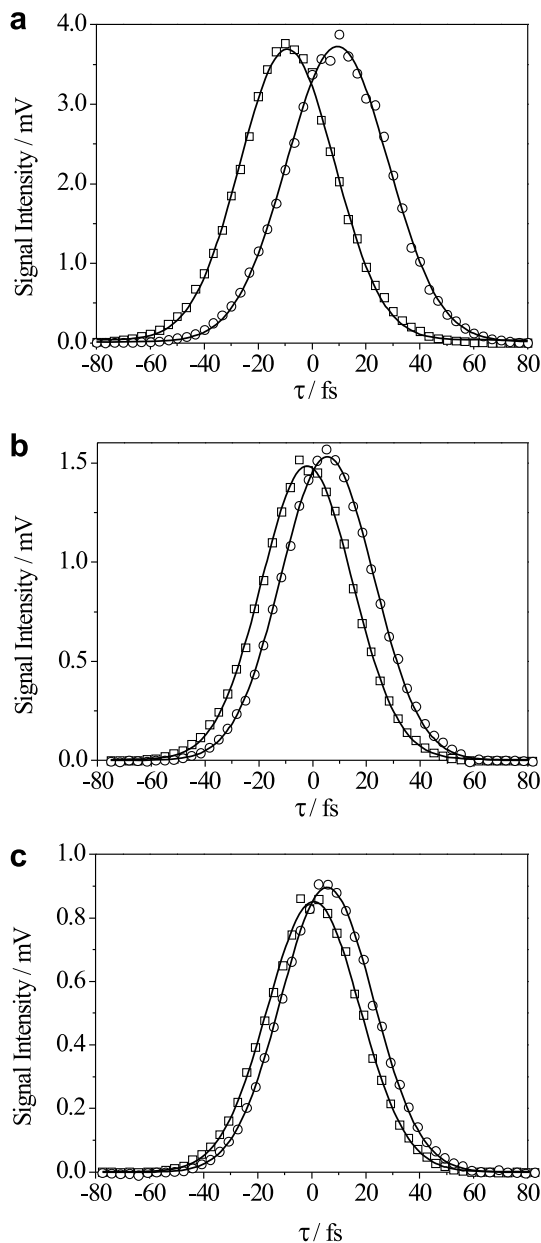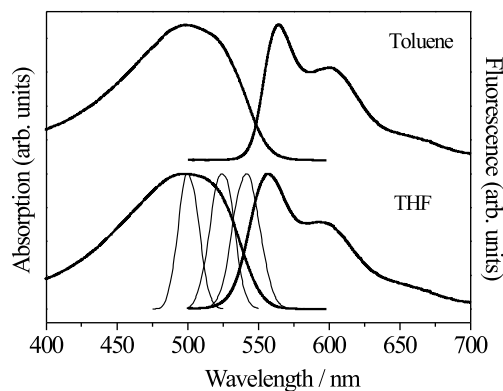
Fig. 2. Three-pulse photon-echo signal intensities for MEH-PPV in toluene (central excitation wavelength at 540 nm) in the phase-matching directions $k_s = -k_1 + k_2 + k_3$ (○) and $k'_s = k_1 - k_2 + k_3$ (□) for population times (a) $T = 0$ fs, (b) $T = 100$ fs, and (c) $T = 500$ fs. Solid lines are Gaussian fits of the data (note that the signal intensities are not scaled).

Fig. 3. Steady-state absorption and time-integrated fluorescence spectra of MEH-PPV in toluene (upper curves) and THF (lower curves). Thin solid lines are excitation pulse spectra with central wavelengths of 500, 525, and 540 nm, respectively.

4. Results

Fig. 3 shows the steady-state absorption and fluorescence spectra (the latter recorded for pulsed excitation at $\lambda_{exc} = 520$ nm) of MEH-PPV in toluene and THF.

At first inspection, the spectra appear quite similar in both solvents, featuring a broad and structureless absorption band, typical for poly(arylenevinylene)-type polymers, and a more resolved emission spectrum, which is shifted considerably to the red. The fluorescence spectra show a progression with two maxima, with an energy spacing of ≈ 1100 cm^{-1}, the precise values being sample dependent. The low-intensity fluorescence band in the very red is not part of the apparent vibronic progression, and may resemble coupling to other than the predominant vibration(s) or the pres-

ence of other emissive species, formed, e.g., upon inter-chain aggregation [22]. The spectral widths of our excitation pulses are approximately 25 nm (full width at half maximum), which allows, at a reasonable balance of experimental resolution in energy and time, excitation into the maximum ($\lambda_{exc} = 500$ nm), the low-energy shoulder ($\lambda_{exc} = 525$ nm), and the far red-wing of absorption ($\lambda_{exc} = 540$ nm, cf. Fig. 3). The corresponding 3-PEPS and TG signals are shown in the left and the right panel of Fig. 4a (THF) and Fig. 4b (toluene), respectively.

In both solvents, initial peak-shifts (τ^*-values for population time $T = 0$) range from 6 to 8 fs, and show a weak trend only to increase at lower excitation energies. On the other hand, the dependence of 3-PEPS signal decays on the chosen excitation energy is quite pronounced, in particular on the early picosecond timescale. For the highest excitation energy, the peak-shifts decrease to a value below 1 fs within about 40 fs, and can be described by a single exponential decay and a small static offset (cf. Table 1). For the two lower excitation energies, the short decay time becomes gradually less dominant, and the 3-PEPS signals feature a second, slower decay component of increasing amplitude (cf. also insets in Fig. 4, left panel). This trend is accompanied by an overall shift to higher peak-shift values. At all excitation energies, the peak-shifts level off on the early picosecond (ps) timescale, and are found to persist also at longer population time delays in the ps region.

Similar to the peak-shift measurements, the transient grating decays, displayed in the right panel of Fig. 4, also show remarkably little dependence on the chosen solvent. However, while any excitation energy dependence is hardly perceptible in the picosecond region, on the sub-ps timescale, the trend in the TG data is clearly opposed to the one observed in the 3-PEPS decays. Here, at lower excitation energies, the amplitudes of slower decay components decrease significantly (cf. Table 1). Though the present data is quite similar in both solvents, the described features are perceived in toluene more explicitly. In particular, this is valid for the weak oscillatory components in both 3-PEPS and TG signals (discussed in more detail at the end of Section 5). We note that the fits presented in Table 1 are given with the intention to quantify the dynamics on the sub-ps timescale, but do not relate to a particular model. Under our experimental conditions, no changes in the signal trends upon variation of excitation densities are observed.

5. Discussion

We start the discussion with the ultrafast (≈ 20–30 fs) decay components observed in the 3-PEPS signal (cf. t_1-values in the 3-PEPS fits in Table 1), for which our measurements indicate a
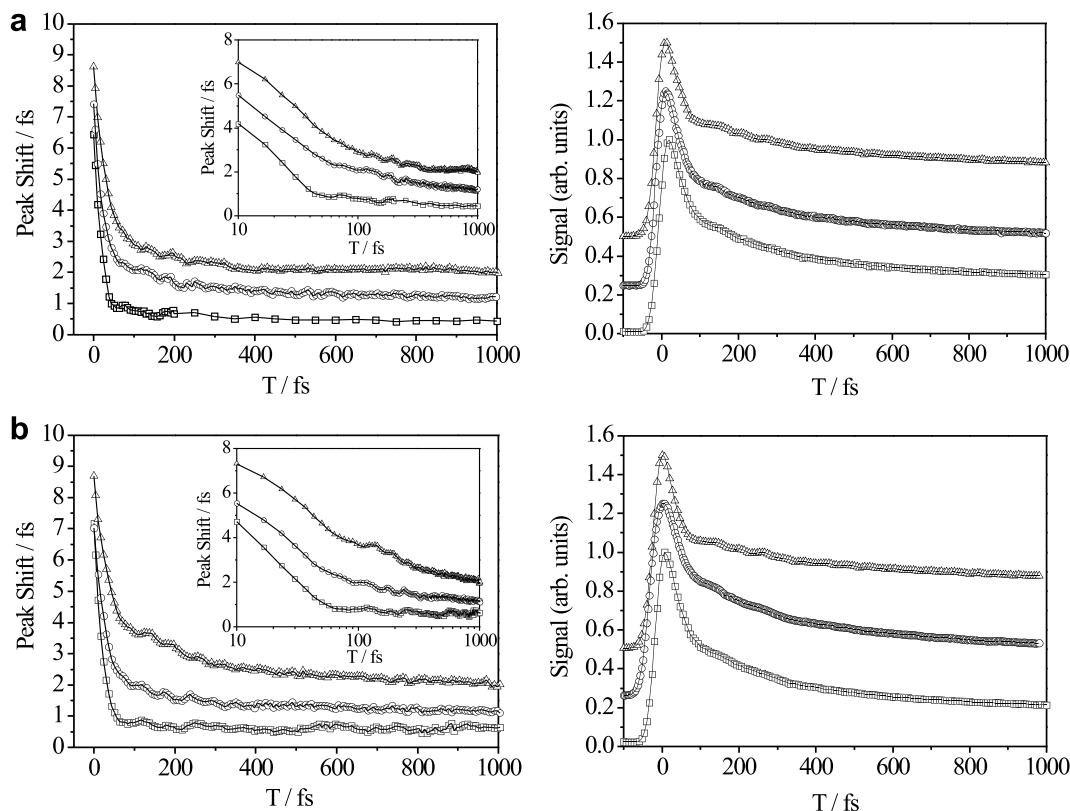
Fig. 4. Three-pulse photon-echo peak-shifts (left panel) and normalized transient grating decays (right panel) for MEH-PPV in (a) THF and (b) toluene, recorded at a central excitation wavelength set to 500 nm ($\square$), 525 nm ($\bigcirc$), and 540 nm ($\triangle$), respectively.

Table 1
Results from mono- ($A_1 \exp[-t/t_1] + A_0$) and bi-exponential ($A_1 \exp[-t/t_1] + A_2 \exp[-t/t_2] + A_0$) fits of 3-PEPS and normalized TG decays in THF (upper panel) and toluene (lower panel)

λ_{exc} (nm)	3-PEPS				TG		
	t_1 (fs)	t_2 (fs)	A_1/A_2	A_0 (fs)	t_1 (fs)	t_2 (fs)	A_1/A_2
THF							
540	26.5 ± 0.8	146 ± 9	3.29	2.06 ± 0.01	24.2 ± 1.1	325 ± 12	2.86
525	19.4 ± 0.5	202 ± 10	3.51	1.22 ± 0.01	26.5 ± 0.7	289 ± 5	2.41
500	19.4 ± 0.7	–	–	0.61 ± 0.02	27.1 ± 1.0	267 ± 5	2.32
Toluene							
540	26.9 ± 1.1	235 ± 10	1.68	2.05 ± 0.02	20.8 ± 0.8	367 ± 13	2.92
525	26.3 ± 0.7	254 ± 22	5.04	1.17 ± 0.02	26.1 ± 0.8	291 ± 4	2.33
500	20.4 ± 0.3	–	–	0.63 ± 0.01	26.5 ± 0.8	271 ± 4	1.88

systematic deceleration with decreasing excitation energy. Quantum-chemical studies propose the first several tens of femtoseconds as the characteristic timescale for the formation of spectroscopic units [23], i.e. the dynamic localization of excited states on segmental subunits of the conjugated chain, driven by interaction with nuclear degrees of freedom. Experimental support for this notion has been the observation of an ultrafast anisotropy decay component in polarization-resolved pump-probe spectra [24]. In previous 3-PEPS studies, sub-30 fs decay components have been assigned to excitation localization effects, leading to a rapid decrease of the observable inhomogeneity of electronic transition energies [7,8]. Accordingly, our data suggests a deceleration of excitation localization at lower excitation energies. This slowdown can be explained by the decreasing amount of vibrational excess energy experienced by torsional/librational modes that drive the localization on particular sites of the polymer chain. We critically note that the dissection of both 3-PEPS and TG signals at very early population time delays (close to the temporal pulse-widths) is not always clear-cut. Subsuming the signal trends and decay times in Fig. 4 and Table 1, we thus focus on our key finding, which is the excitation energy dependence of the 3-PEPS and TG traces on the ps timescale, accompanied by a strong variation in absolute peak-shift values.

In a conjugated polymer, the delocalization of excitations is restricted by a distribution of segmental sites, which are defined by conjugation defects of the chain that can be assumed to be static on the picosecond timescale. Upon broadband excitation, ultrafast dynamic localization on these spectroscopic units yields a manifold of molecular excitons, localized with regard to the overall physical length of the polymer chain and distributed in space and energy. The subsequent temporal evolution is determined by an interplay of intra-site relaxation and inter-site transfer, mediated by electronic site-to-site couplings. The latter induce the inter-segmental diffusion of excitons along the chain by a hopping-type motion towards lower energies in the density of states. Thereby, the typical timescales of inter-site excitation transfer strongly depend on the

excitation boundaries set by the excitation pulse spectrum [25,26]. This is reflected by the excitation energy dependence of the nonlinear response.

In the high energy region of the density of states, the rates of inter-site energy transfer are high, due to many available acceptors in space and energy. This is further enhanced by the stronger electronic interactions between shorter segments that are preferentially excited at shorter wavelengths [27]. Thus, during population time T, a strong population redistribution between electronic states is caused by a large number of individual relaxation events. Given the dynamic disorder induced by bath-fluctuations at different sites is uncorrelated, excitation energy transfer will generally accelerate the correlation decay, even if the involved states are close to electronic resonance. This leads to a fast decrease of the rephasing capability and the peak-shift amplitudes. Further, at high excitation energies, efficient downhill transfer moves a considerable part of the population rapidly into states that lie beyond the spectrum of the excitation pulse. The spectral diffusion out of the experimental detection window will effectively act as a population decay, enhancing the TG signal decay. The complete absence of a (slow) sub-ps decay component in the 3-PEPS traces for the highest chosen excitation energy ($\lambda_{exc} = 500$ nm) is likely to be caused by additional signal contributions due to vibrational cooling of high frequency modes [19,28]. For $\lambda_{exc} = 500$ nm, the spectral distance from the onset of absorption exceeds the spacing in the fluorescence progression (cf. Fig. 3), and one can expect the excitation pulses to be resonant with overtones of vibrational modes (of low energy sites) that are strongly coupled to the electronic transition.

The number of accessible states within which an exciton can move becomes restricted at lower excitation energies. At the energetic bottom of the density of states, the timescales of inter-site transfer increase, due to the lack of potential acceptors in spatial proximity. The elimination of inter-site coupling effects by selective excitation thus allows to observe the system-bath interaction and (intra-segmental) relaxation of excitations that are essentially site-localized on a ps timescale. The observed correlation decay of transition energies will thus rather reflect the characteristics of the oligomeric sites themselves. In this context, we point to both experimental and theoretical studies that conclude low-frequency torsional modes to play a key-role in the equilibration of photoexcited conjugated segments [29–31]. Since the equilibrium geometries of excited states are more planar as compared to the ground state, electronic excitation induces a conformational change towards smaller torsional angles. The spectral diffusion accompanying such intra-site events can be clearly expected to be smaller than for site-to-site transfer. In fact, at lower excitation energies, we find a deceleration of 3-PEPS signal decays on the early ps timescale, the trend being more pronounced in toluene. For $\lambda_{exc} = 540$ nm (in toluene), apart from the asymptotic off-set, the functional form is even quantitatively comparable to the result reported for a model pentamer [7]. The decay components in the TG signal, in turn, indicate a slowdown in the detected population dynamics of non-interacting sites, congruent with our line of argumentation.

The high sensitivity of 3-PEPS signals to the excitation conditions is underlined by the variation of static peak-shift components by more than a factor of three (cf. A_0-values listed in Table 1). For an ensemble of uncoupled sites, one would expect the contribution of static disorder to the 3-PEPS signal to decrease for excitation energy tuning from the maximum to the edge of the absorption spectrum. Obviously, this is in contrast to what we observe. Rather, our results illustrate that the actual extent of inhomogeneity in the system can be perceived most explicitly at low excitation energies, where the signal decay becomes increasingly less affected by memory loss through inter-segmental relaxation events. The pres-

ence of long-lived 3-PEPS components differentiates the optical response of a conjugated polymer from other excitonic systems. For J-aggregates, e.g., no finite peak-shifts beyond ≈ 100 fs are observed [15,32]. In contrast to the periodic assembly of identical dye molecules forming an aggregate, in a conjugated polymer, random conjugation breaks form an uncorrelated ensemble of segmental sites, that will be additionally subject to torsional disorder. The consequently broad spatio-energetic distribution of spectroscopic units gives rise to the pronounced peak-shift offset, observable at low excitation energies.

Despite the large difference in the dipole moments of the two solvents ($\mu_{Tol} = 0.37$ D, $\mu_{THF} = 1.75$ D [33]), the 3-PEPS and TG data sets are quite similar at high excitation energies. Only for $\lambda_{exc} = 540$ nm, the 3-PEPS decay in toluene is distinctly decelerated as compared to THF. According to the arguments outlined above, in this regime the non-linear signals are most sensitive to site-specific characteristics. From measurements of the hydrodynamic radii, it has been concluded that MEH-PPV tends to unfold in aromatic solvents, due to π–π interactions with the polymer backbone [22]. Qualitatively, a tighter coiling (as in THF) should increase the efficiency of site-to-site energy transfer. On the other hand, a more spread geometry will additionally reduce the steric repulsion between the branched side chains and allow for an increase of the average unbroken π-conjugation length. Lower-energy segments will undergo a reduced configurational change in the excited state, and further slow down the 3-PEPS decay. Overall, our data (for $\lambda_{exc} = 540$ nm) might reflect a difference in effective conjugation lengths, induced by a change of the solvent.

We finally turn to the oscillatory features observed in both types of non-linear signals. Fig. 5a shows the Fourier-transforms of
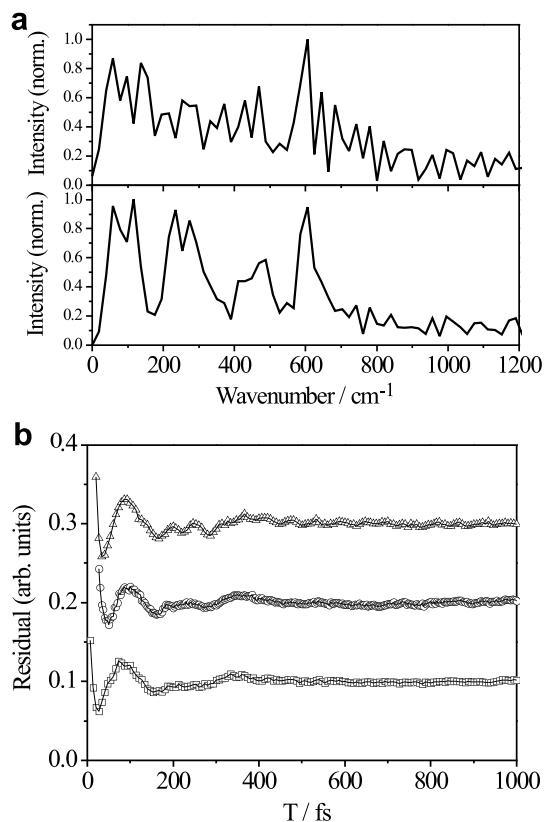
Fig. 5. (a) Fourier transforms of the oscillatory components in 3-PEPS (top panel) and transient grating (lower panel) data of MEH-PPV in toluene ($\lambda_{exc} = 540$ nm). (b) Residuals to bi-exponential fitting of transient grating decays in toluene, recorded at a central excitation wavelength set to 500 nm ($\square$), 525 nm ($\bigcirc$), and 540 nm ($\triangle$), respectively.

3-PEPS and TG decays in toluene solution for $\lambda_{exc} = 540$ nm, after subtraction of bi-exponential fits to remove slowly decaying components. While the spectral intensities in the region below 400 cm^{-1} originate from low frequency noise that is not eliminated by exponential fitting, the spectral feature around 600 cm^{-1} is reproducible under all experimental conditions, and, though less pronounced, is observed in THF as well. Fig. 5b shows residues to bi-exponential fits of TG decays in toluene for all three excitation wavelengths. The oscillations are damped out on a timescale of 200 fs, with modulation depths increasing for lower excitation energies.

While high frequency modes of poly(phenylenevinylene) (PPV) derivatives have been studied with considerably shorter pulses [34–36] (<10 fs), the weak low-frequency beating observed in the present study is somewhat surprising, and has not been reported in previous photon-echo studies [7,8]. The observation of oscillating signal components is intriguing, since it has been argued that vibrational coherence effects should be washed out in a congested vibrational manifold. We stress that a comparative study of infrared (IR) and Raman spectra of PPV and several of its oligomeric model compounds indicates a low sensitivity of IR/Raman frequencies to the conjugation length; rather, the bands rapidly converge to those of the polymer chain [37]. It is therefore not unreasonable to assume at least weak vibronic modulations in our signals, although the unambiguous assignment to a particular mode on the basis of available IR/Raman spectra [37–40] turns out to be arduous. For PPV, a strong infrared mode around 550 cm^{-1} is assigned to a combined C–H/(C–C)$_{ring}$ out-of-plane bending and any Raman modes below 1000 cm^{-1} are very weak only [39]. However, this mode is not reported for MEH-PPV, for which the IR spectrum suggests a band at 700 cm^{-1} (assigned to O–CH$_2$ rocking motion) as the only reasonable candidate [40]. Comparing other IR/Raman frequencies, we find no convenient explanation in terms of a difference or sum frequency beating. Certainly, these difficulties partly arise from the low modulation amplitude, which limits the accuracy in determination of the underlying frequency. We suggest that pump-probe detection schemes, specifically designed to enhance low-frequency vibrational coherence signals [41,42], should be useful to clarify this puzzle. It is worth mentioning that oscillations in 3-PEPS signals that result from electronic rather than vibrational coherences have received considerable attention recently [43,44]. Though the chance to observe electronic coherences in a conjugated polymer increases for energetic bottom states [45,46], it is too speculative to draw a straightforward analogy with the present data.

In summary, for high excitation energies, we conclude the third-order nonlinear signals to be dominated by exciton redistribution during population time *T*. This observation is basically in line with results of Scholes and co-workers [7,8], who concluded that site-to-site coupling effects need to be accounted for in a description of the MEH-PPV lineshape. We can add that, as a consequence, excitation energies in 3-PEPS/TG experiments have to be chosen carefully, as the extent of static inhomogeneity in the spectral lineshape of MEH-PPV can be observed in an unbiased fashion at low excitation energies only.

References

[1] N.S. Sariciftci, Primary Photoexcitations in Conjugated Polymers: Molecular Exciton vs. Semiconductor Band Model, World Scientific, Singapore, 1997.
[2] H. Bässler, B. Schweitzer, Acc. Chem. Res. 32 (1999) 173.
[3] S. Mukamel, D. Abramavicius, Chem. Rev. 104 (2004) 2073.
[4] S. Mukamel, Principles of Nonlinear Optical Spectroscopy, Oxford University Press, Oxford, 1995.
[5] T.A. Pham, A. Daunois, J.-C. Merle, J.L. Moigne, J.-Y. Bigot, Phys. Rev. Lett. 74 (1995) 904.
[6] G.D. Scholes, D.S. Larsen, G.R. Fleming, G. Rumbles, P.L. Burn, Phys. Rev. B 61 (2000) 13670.
[7] X. Yang, T.E. Dykstra, G.D. Scholes, Phys. Rev. B 71 (2005) 45203.
[8] T.E. Dykstra, V. Kovalevskij, X. Yang, G.D. Scholes, Chem. Phys. 318 (2005) 21.
[9] S. Mukamel, R.F. Loring, J. Opt. Soc. Am. B 3 (1986) 595.
[10] W.P. de Boeij, M.S. Pshenichnikov, D.A. Wiersma, J. Phys. Chem. 100 (1996) 11806.
[11] T. Joo, Y. Jia, J.-Y. Yu, M.J. Lang, G.R. Fleming, J. Chem. Phys. 104 (1996) 6089.
[12] K.F. Everitt, E. Geva, J.L. Skinner, J. Chem. Phys. 114 (2001) 1326.
[13] W.P. de Boeij, M.S. Pshenichnikov, D.A. Wiersma, Annu. Rev. Phys. Chem. 49 (1998) 99.
[14] G.R. Fleming, M. Cho, Annu. Rev. Phys. Chem. 47 (1996) 109.
[15] K. Ohta, M. Yang, G.R. Fleming, J. Chem. Phys. 115 (2001) 7609.
[16] W.M. Zhang, T. Meier, V. Chernyak, S. Mukamel, J. Chem. Phys. 108 (1998) 7763.
[17] W.M. Zhang, T. Meier, V. Chernyak, S. Mukamel, Phil. Trans. R. Soc. Lond. A 356 (1998) 405.
[18] J. Piel, E. Riedle, L. Gundlach, R. Ernstorfer, R. Eichberger, Opt. Lett. 31 (2006) 1289.
[19] K. Ohta, D.S. Larsen, M. Yang, G.R. Fleming, J. Chem. Phys. 114 (2001) 8020.
[20] P. Baum, S. Lochbrunner, E. Riedle, Opt. Lett. 29 (2004) 210.
[21] P. Baum, E. Riedle, J. Opt. Soc. B 22 (2005) 1875.
[22] T. Nguyen, V. Doan, B.J. Schwartz, J. Chem. Phys. 110 (1999) 4068.
[23] W.J.D. Beenken, T. Pullerits, J. Phys. Chem. B 108 (2004) 6164.
[24] M.M.-L. Grage, Y. Zaushitsyn, A. Yartsev, M. Chachisvilis, V. Sundström, T. Pullerits, Phys. Rev. B 67 (2003) 205207.
[25] J. Sperling, F. Milota, A. Tortschanoff, C. Warmuth, B. Mollay, H. Bässler, H.F. Kauffmann, J. Chem. Phys. 117 (2002) 10877.
[26] J. Sperling, C. Benesch, L. Kuna, H.F. Kauffmann, F. Milota, Synt. Met. 143 (2004) 315.
[27] S. Westenhoff, W.J.D. Beenken, R.H. Friend, N.C. Greenham, A. Yartsev, V. Sundström, Phys. Rev. Lett. 97 (2006) 166804.
[28] D.S. Larsen, K. Ohta, Q.-H. Xu, M. Cyrier, G.R. Fleming, J. Chem. Phys. 114 (2001) 8008.
[29] S. Karabunarliev, E.R. Bittner, M. Baumgarten, J. Chem. Phys. 114 (2001) 5863.
[30] W.J.D. Beenken, H. Lischka, J. Chem. Phys. 123 (2005) 144311.
[31] V. Lukes, A.J.A. Aquino, H. Lischka, H.F. Kauffmann, J. Phys. Chem. B 111 (2007) 7954.
[32] J.-H. Lee, C.-K. Min, T. Joo, J. Chem. Phys. 114 (2001) 377.
[33] D.R. Lide (Ed.), Handbook of Chemistry and Physics, 86th ed., CRC Press, 2005.
[34] G. Cerullo, G. Lanzani, L. Pallaro, S. De Silvestri, J. Mol. Struct. 521 (2000) 261.
[35] G. Lanzani, G. Cerullo, S. Stagira, M. Zavelani-Rossi, S. De Silvestri, Synt. Met. 119 (2001) 491.
[36] G. Lanzani, G. Cerullo, C. Brabec, N.S. Sariciftci, Phys. Rev. Lett. 90 (2003) 47402.
[37] A. Sakamoto, Y. Furukawa, M. Tasumi, J. Phys. Chem. 96 (1992) 1490.
[38] Y. Furukawa, A. Sakamoto, M. Tasumi, J. Phys. Chem. 93 (1989) 5354.
[39] D. Rakovic, R. Kostic, L.A. Gribov, I.E. Davidova, Phys. Rev. B 41 (1990) 10744.
[40] K.F. Voss, C.M. Foster, L. Smilowitz, D. Mihailovic, S. Askari, G. Srdanov, Z. Ni, S. Shi, A.J. Heeger, F. Wudl, Phys. Rev. B 43 (1991) 5109.
[41] F. Rosca, D. Ionascu, A.T.N. Kumar, A.A. Demidov, P.M. Champion, Chem. Phys. Lett. 337 (2001) 107.
[42] F. Rosca, A.T.N. Kumar, D. Ionascu, T. Sjodin, A.A. Demidov, P.M. Champion, J. Chem. Phys. 114 (2001) 10884.
[43] H. Lee, Y.C. Cheng, G.R. Fleming, Science 316 (2007) 1462.
[44] P. Kjellberg, T. Pullerits, J. Chem. Phys. 124 (2006) 24106.
[45] F. Milota, J. Sperling, A. Tortschanoff, V. Szöcs, L. Kuna, H.F. Kauffmann, J. Lum. 108 (2004) 205.
[46] F. Milota, J. Sperling, V. Szöcs, A. Tortschanoff, H.F. Kauffmann, J. Chem. Phys. 120 (2004) 9870.